Plasma Physics Reports, Vol. 24, No. 7, 1998, pp. 556–563. Translated from Fizika Plazmy, Vol. 24, No. 7, 1998, pp. 603–610.

LOW-TEMPERATURE PLASMA

Generation of Cold Electrons in a Low-Pressure RF Capacitive Discharge as an Analog of a Thermal Explosion

S. V. Berezhnoi, I. D. Kaganovich, and L. D. Tsendin

St. Petersburg State Technical University, ul. Politekhnicheskaya 29, St. Petersburg, 195251 Russia

Received October 22, 1997; in final form, February 26, 1998

Abstract—Theoretical analysis of the formation of a two-temperature electron distribution function in a low-pressure rf capacitive discharge is presented. A transition to a peaked profile of the electron distribution function as the current increases is studied. Calculations and experiments show that, as the current increases, a radical rearrangement of the electron distribution accompanied by the formation of a two- temperature distribution function can occur. As a result, the average electron energy strongly decreases. For a current density above the critical value, a steady-state solution can be obtained only if the electron–electron collisions are taken into account. The transition mechanism is similar to that for a thermal explosion.

1. INTRODUCTION

Radio-frequency capacitive (RFC) discharges are widely used in industry for plasma etching, film deposition, etc. Interest in studying RFC discharges is motivated, in particular, by the problem of the formation of a strongly non-Maxwellian electron distribution function (EDF) at low pressures [1].

Since the EDF can be far from Maxwellian, it is necessary to solve the kinetic equation for electrons even for a qualitative description of RFC discharges.

A self-consistent analysis of an intricate structure of the RFC discharge should involve numerical simulations. Quite a number of approaches were used to solve this problem; however, the existing methods for simulation of a RFC discharge require a very large computational expenditure. This makes it difficult to perform calculations over a wide range of parameters, obtain scalings, and predict the effect of such external factors as pressure, current, field frequency, etc. on the discharge parameters.

The computation time can be strongly decreased by using the optimum combination of numerical and analytical methods. Such an approach was used in [2] to describe an RFC low-pressure discharge.

RFC discharge can be completely described by a self-consistent set of nonlinear nonsteady equations including kinetic equation for electrons, the Poisson equation, and the equation of continuity for the ions. Their temporal and spatial scales are very different, which makes simulations extremely complicated. By using a nonlocal approximation, splitting the discharge gap into the region of a quasineutral plasma and the region of the ion space charge (which does not contain electrons), and averaging the solution over the fast electron motion, the authors of [2] excluded small temporal and spatial scales. A derivation of the set of equations is presented in [2, 3]. Based on these equations, it is possible to perform fast simulation (FS) of a RFC discharge. For a simple atomic gas, one personal-computer run takes about 10 min, whereas Monte Carlo simulations on a supercomputer require at least several hours. The applicability of the set of equations used in FS is proved in [3–5] by comparing the results of FS with those of calculations based on the full set of equations. Comparison of the FS results with experimental data and an analysis of forming the EDF are presented in [3].

In this paper, we consider the formation of a two-temperature EDF caused by the nonlocal character of the process, a transition to the peaked EDF profile as the current increases, the characteristic features of this transition, and the reasons for its occurrence.

Using a non-self-sustaining discharge as an example, we show that the mechanism for the instability of the discharge that results in the formation of a peak of cold electrons in the EDF is very similar to the mechanisms governing the thermal explosion.

The thermal explosion, i.e., the process characterized by the absence of a steady-state temperature profile, at which the thermal sources are balanced by heat removal, usually occurs because of the exponential dependence of the heat release $Q(T)$ on temperature [6]. In a region with size $2L$, the steady-state equation of thermal conduction is

$$\frac{d}{dx}\left(\chi(T)\frac{d}{dx}T(x)\right)+Q(T) = 0,\qquad T(x = 0, L) = 0. \tag{1}$$

The thermal explosion implies that, for L above a certain critical size L_{cr}, there are no solutions to equation (1). For $Q(T) = Q_0\exp(\alpha T)$ and $\chi = \text{const}$, the critical size is $L_{cr} = 1.88\sqrt{\chi/(Q_0\alpha)}$. The reason for the thermal explosion is that heat transfer that is proportional to the temperature at the center of the gap ($\chi T_0/L$) cannot carry away heat released with the rate $Q_0\exp(\alpha T)$. It is easily seen that equation (1) with a nonlinear thermal conductivity $\chi(T)$ can possess the same property.

If thermal conductivity $\chi(T)$ decreases with increasing temperature, heat self-trapping can occur. The heat flux is determined by an integral of the volume sources

$$-\chi(T)\frac{dT}{dx} = \int_0^x Q(x')dx'. \tag{2}$$

For homogeneous heat release, we have

$$\int_0^{T_0}\chi(T)dT = Q_0L^2/8. \tag{3}$$

For $T_0 \longrightarrow \infty$, integral in the left-hand side of (3) can converge, for example, if

$$\chi \sim (T+T_1)^{-\beta}, \tag{4}$$

where $\beta > 1$ and T_1 are constants. This implies that the temperature growth leads to an improvement in heat insulation, and, for

$$L^2 > L_{cr}^2 = 8\int_0^\infty \chi(T)dT/Q_0 \tag{5}$$

heat self-trapping occurs.

RFC discharges possess similar properties. As the plasma density increases, the role of electron heating in sheaths becomes greater, and the temperature of the bulk electrons decreases. Correspondingly, the steady-state ambipolar electric field and the ambipolar diffusion coefficient also decrease, which improves the plasma confinement. In a self-sustaining discharge, the generation of particles intricately depends on the fields and, accordingly, on the plasma density profile. Therefore, the inverse effect of the plasma profile on both the plasma source and the outward plasma motion is significant.

In order to better understand the above mechanism, which is caused by the density effect on the particle transport, we study a simple case of a non-self-sustaining discharge, when the particle source is determined by external ionization, and the inverse effect of the plasma density on the plasma losses is most pronounced.

2. EQUATIONS FOR FAST SIMULATION

2.1. Basic Statements

We consider a RFC discharge in the plane geometry at pressures $0.01 \lesssim p \lesssim 0.1$ torr, when collisions are essential. The schematic of the discharge is presented in Fig. 1.

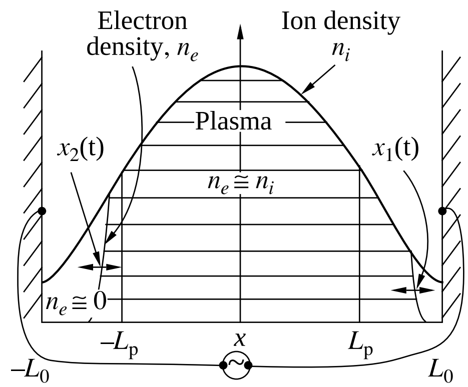

Fig. 1. Schematic of the RFC discharge.

The basic statements of the theory developed in [2] are the following:

(i) The discharge consists of two regions: the region of quasineutral plasma and the region of a space charge shielding the voltage applied to the capacitor (Figs. 1 and 2). The shielding condition is $\omega_{0e} \gg \max(\sqrt{\nu\omega}, \omega)$, where ω_{0e} is the plasma electron frequency, ω is the frequency of the rf field, and ν is the frequency of elastic electron–atom collisions.

(ii) Since the amplitude of the applied voltage is $U(\sim 10\text{–}1000$ B) $\gg T_e/e(\sim 1$ V), the sheath thickness $L_{sh} \sim r_D\sqrt{eU/T_e}$ is far above the thickness the transition region (on the order of the Debye radius r_D) between the neutral plasma and the region of an ion space charge. Further, we will refer to this transition region as the plasma–space-charge boundary. We assume that the potential drop at this boundary is fairly high, so that it prevents electrons from penetrating into the region of the ion space charge; the reflection of electrons from the boundary potential wall is absolutely elastic. Figure 2 shows the motion of the sharp plasma–space-charge boundary. The boundary position as a function of $Z \equiv \omega t$ is presented by the lines $x_{1,2}(\omega t)$; some part of the rf-field period, the sheath is in the plasma phase, and the other part, it is in the phase of a space charge. In Figure 2, the plasma phase is shown in coordinates $\{x, t\}$ by a single-hatched domain.

(iii) The electric field is described in different ways in different regions of the discharge. In the sheath region, we solve the Poisson equation, and, for the space- charge field, we have [7–9]

$$E(x,t) = \frac{4\pi j_0}{\omega}(\cos(\omega t) - \cos(Z_{1,2}(x))), \tag{6}$$

where $j(t) = -j_0\sin(\omega t)$ is the total density of the current flowing through the discharge, functions $Z_{1,2}(x)$ are the functions inverse to $x_{1,2}(\omega t)$, and the current in the space-charge phase is the displacement current. We assume the condition $\omega_{0i} \ll \sqrt{\nu_i\omega}$ to hold, where ω_{0i} is

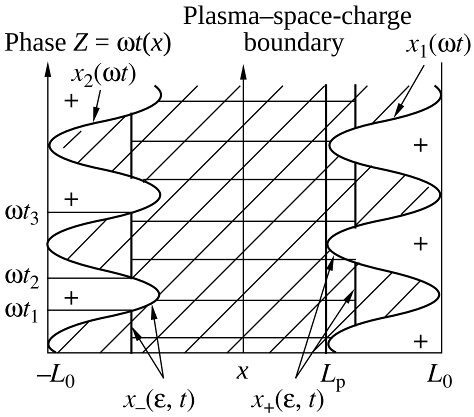

Fig. 2. Schematic of the motion of the plasma–space-charge boundary (single-hatched plasma region) and schematic of the region accessible for electrons with the total energy ε (double-hatched region).

the plasma ion frequency and ν_i is the frequency of elastic ion–atom collisions. The displacement of ions during the rf-field period is small compared to the sheath thickness, and the ion density profile can be considered steady-state during this period [10, 11].

In the plasma (i.e., for $|x| < L$, where L_p is the position of the plasma–sheath boundary) and in the sheath in the plasma phase, the field can be represented as a sum of the oscillating part $\tilde{E}(x, t)$ and time-independent part $\bar{E}(x)$ (averaged over the rf-field period): $E(x, t) = \tilde{E}(x, t) + \bar{E}(x)$. The field $\bar{E}(x)$ in plasma is defined as

$$\bar{E}(x) = \frac{\omega}{2\pi}\int_0^{\omega/2\pi} E(x, t)dt \equiv -\frac{d\Phi}{dx}, \tag{7}$$

and the oscillating part is determined from

$$j(t) = \sigma\tilde{E}(x, t). \tag{8}$$

The field $\tilde{E}(x, t)$ is responsible for the Ohmic heating, and $\bar{E}(x)$ is the steady-state ambipolar field that draws ions from the plasma and prevents electrons from escaping the plasma. In the sheath, the averaging is performed over the time interval $t_2 < t < t_3$ (see Fig. 2) during which the sheath is in the plasma phase:

$$E(x, t) = \tilde{E}(x, t) + \bar{E}(x),$$
$$\bar{E}(x) = \frac{1}{t_3 - t_2}\int_{t_2}^{t_3} E(x, t)dt \equiv -\frac{d\Phi}{dx}. \tag{9}$$

2.2. Kinetic Equation for Electrons

We consider an RFC discharge at a low pressure when the length λ_ε of the electron energy relaxation exceeds the length $2L_0$ of the discharge gap. As a rule, the energy relaxation length is minimum for electrons from the EDF tail, for which this length is determined by inelastic collisions. There λ_ε can be estimated as $\sqrt{\lambda\lambda^*/3}$, where λ, λ^* are the mean free paths of electrons with respect to elastic and inelastic collisions, respectively. We assume $\lambda \ll L_{sh}$, which permits us to neglect the collisionless heating. For $\lambda \ll L_0, \lambda^*$, a two-term approximation $f(x, \mathbf{v}, t) = f_0(v, x, t) + f_1(v, x, t)\cos\theta$ can be used to solve the kinetic equation. Here, θ is the angle between the direction of the electron motion and the electric field. The anisotropic part of the EDF is assumed to be small ($f_1 \ll f_0$) [12]. For inert gases $\lambda/\lambda^* \sim 10^1$–$10^2$.

After we divided the field into the oscillating and time-independent parts, it is possible to introduce a new variable, namely, the total energy $\varepsilon = mv^2/2 + e\Phi(x)$ [2] and to pass to the variables $\{\varepsilon, x, t\}$. For $\lambda_\varepsilon \gg L_0$, the total energy of an electron remains almost unchanged during its motion in the potential well between turning points $x_-(\varepsilon, t)$ and $x_+(\varepsilon, t)$ (the double-hatched domain in Fig. 2), and, from the condition $\omega \gg \nu^*$, it follows that the EDF is steady-state [13]. Thus, $f_0(\varepsilon, x, t) \approx F_0(\varepsilon)$, i.e., the EDF is primarily a function of the total energy alone. The time- and space-dependent corrections to $F_0(\varepsilon)$ are on the order of (ν^*/ω) and $(L_0/\lambda_\varepsilon)^2$, respectively.

The kinetic equation averaged over the rf-field period and coordinate (over the region accessible for electron with the given total energy) has the form [2]

$$\frac{d}{d\varepsilon}\left(\overline{vD_\varepsilon}(\varepsilon)\frac{dF_0(\varepsilon)}{d\varepsilon}\right) = \sum_k \overline{v\nu_k^*}(\varepsilon)F_0(\varepsilon) - \sum_k \overline{v\nu_k^*}(\varepsilon + \varepsilon_k^*)F_0(\varepsilon + \varepsilon_k^*), \tag{10}$$

where the coefficient of diffusion of electrons by energy is

$$vD_\varepsilon(v, x, t) = \cos^2(\omega t)e^2v^3\tilde{E}^2(x, t)\nu/(3(\omega^2 + \nu^2)), \tag{11}$$

ν and ν_k^* are the frequencies of the elastic transport collisions and inelastic collisions, respectively; and ε_k^* is the threshold for inelastic collisions. The averaging operator is

$$\overline{G(v, x, t)} \equiv \bar{G}(\varepsilon) = \frac{1}{2L_0 T}\int_0^T dt \times \int_{x_-(\varepsilon, t)}^{x_+(\varepsilon, t)} G\left(\sqrt{\frac{2}{m}[\varepsilon - e\Phi(x)]}, x\right) dx. \quad (12)$$

The kinetic equation (10) takes into account the ohmic heating and inelastic losses of electrons.

2.3. Continuity Equation for Ions

For $\omega_{0i} \ll \sqrt{\nu_i \omega}$, the ion density profile can be described by the continuity equation averaged over the rf-field period

$$\frac{\partial n_i \langle u_i \rangle}{\partial x} = \langle I(x, t) \rangle, \quad (13)$$

where $I(x, t)$ is the ionization source, and the angular brackets denote time- averaging.

Assuming the free path λ_i of ions to be small compared to L_{sh} and L_0 and the condition $\omega \gg \nu_i$ to hold, it is possible to solve the time-averaged kinetic equation for ions and to obtain the expression for the average ion velocity. For the cross section of elastic ion–atom collisions $\sigma_{ia} = \sigma_0 v^\beta$ (with $-1 \le \beta \le 0$), the average ion velocity is

$$u_i = \pm\left(\frac{4e(\beta + 2)}{MN_a\sigma_0}\right)^{1/(2+\beta)} \frac{1}{2\sqrt{\pi}} \times \Gamma\left(\frac{4+\beta}{2(2+\beta)}\right) |\langle E(x, t)\rangle|^{1/(2+\beta)}, \quad (14)$$

where Γ is gamma-function, M is the ion mass, N_a is the density of neutral atoms, and $\langle E(x, t)\rangle$ is the electric field averaged over the rf-field period; the plus sign in (14) corresponds to the right-hand sheath, and the minus sign corresponds to the left-hand one.

According to the field representation described above, the field $\langle E(x, t)\rangle$ includes both the ambipolar field $-(d\Phi(x)/dx)$ and the averaged field of the space charge (6)

$$\langle E(x, t)\rangle = -\frac{d\Phi}{dx}(1 - Z(x)/\pi) \pm \frac{4j_0}{\omega}[\sin(Z(x)) - Z(x)\cos(Z(x))]. \quad (15)$$

In plasma, we have $Z = 0$, and $\langle E(x, t)\rangle$ coincides with the ambipolar field.

2.4. Complete Set of Equations

In order to close the set of equations, it is necessary to relate the electron density, conductivity, and ionization cross section with the EDF

$$n_e(x) = \frac{4\pi}{m}\int_{e\Phi(x)}^{\infty} F_0(\varepsilon)\sqrt{\frac{2}{m}(\varepsilon - e\Phi(x))}\, d\varepsilon, \quad (16)$$

$$\sigma = \frac{8\pi e^2}{3m^2}\int_{e\Phi(x)}^{\infty} v\frac{\varepsilon - e\Phi(x)}{\nu + i\omega}\frac{dF_0}{d\varepsilon}d\varepsilon, \quad (17)$$

$$\langle I(x, t)\rangle = \left(1 - \frac{Z(x)}{\pi}\right)\frac{4\pi\sqrt{2}}{m^{3/2}} \times \int_{e\Phi(x)+\varepsilon_I}^{\infty} [N_a v \sigma_{\text{ion}}(\varepsilon - e\Phi(x))] F_0(\varepsilon)\sqrt{\varepsilon - e\Phi(x)}\, d\varepsilon, \quad (18)$$

where σ_{ion} is the ionization cross section, and ε_I is the energy threshold for ionization.

The quasineutrality condition determines the ambipolar potential in the plasma and sheath (in the plasma phase)

$$\frac{4\pi}{m}\int_{e\Phi(x)}^{\infty} F_0(\varepsilon)\sqrt{\frac{2}{m}(\varepsilon - e\Phi(x))}\, d\varepsilon = n_i(x). \quad (19)$$

The boundary conditions for the potential are $\Phi|_{x=0} = 0$ and $(d\Phi/dx)|_{x=0} = 0$.

The obtained set of equations does not contain small temporal and spatial scales and permits FS of the RFC discharge.

2.5. Numerical Scheme

We start calculations with a certain initial EDF and arbitrary profile of the ion density. The potential $\Phi(x)$ is determined from equation (19). The execution cycle for ions corresponds to solution of the equation of continuity for ions (13) using the relaxation method and assuming fixed EDF. In every cycle, we use a new profile of the ion density and find the new ambipolar potential. After completing the ion cycle, we calculate the amplitude of the oscillating conduction field by using equations (8) and (17), new values of the potential $\Phi(x)$ and ion density $n_i(x)$, and the previous EDF. A new EDF is found from kinetic equation (10) with new coefficients (11) and (12). Cycles for calculation of the EDF together with ion cycles are repeated until a steady-state solution establishes.

For a simple atomic gas, the solution of the set of equations takes on the order of 10 min personal-computer time.

The presented scheme allows us to describe the physical processes occurring in the system on characteristic ion time scales and permits investigation of

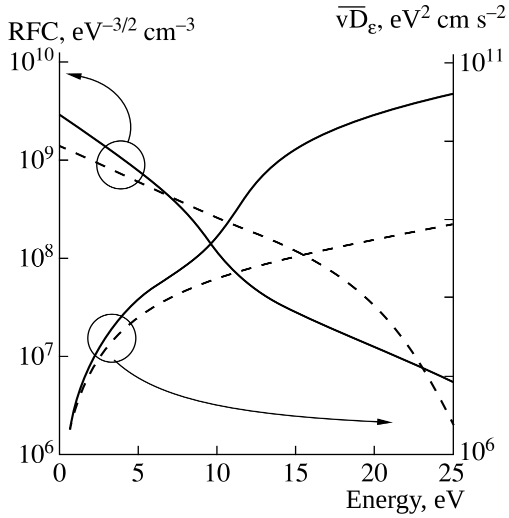

Fig. 3. The results of fast simulation for helium, $p = 0.1$ torr, $L_0 = 3.35$ cm, $\omega = 13.56$ MHz, and $j_0 = 8.8$ mA/cm^2. The solid line corresponds to calculation using the nonlocal approximation, and the dashed line is the result obtained in the local approximation (see the text).

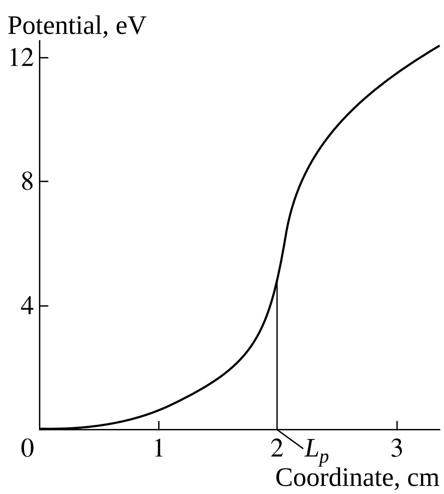

Fig. 4. The results of fast simulation for helium, $p = 0.1$ torr, $L_0 = 3.35$ cm, $\omega = 13.56$ MHz, and $j_0 = 8.8$ mA/cm^2. Ambipolar potential calculated with the use of the nonlocal approximation (see the text and Fig. 3); L_p is the plasma–sheath boundary.

temporal evolution of the system with a time step on the order of characteristic time of ion loss from the sheath.

3. RESULTS OF CALCULATIONS

3.1. Formation of a Peak of Cold Electrons in the EDF due to a Nonlocal Character of the Process

The formation of a peak of cold electrons in the EDF was investigated in [5]. For a sufficiently high current, when the difference between ion densities in the center of the gap and at the periphery is large, nonlocal character of the process results in enriching the low-energy part of the EDF.

In this case, the electrons can be divided into two groups. Electrons with $\varepsilon < e\Phi_{sh} = e\Phi(L_p)$ are trapped in the region of a low heating field ($\tilde{E}_0(x) \sim 1/n(x)$), whereas electrons with $\varepsilon > e\Phi_{sh}$ can (in the plasma phase) penetrate into the sheath, in which the amplitude of the oscillating conduction field $\tilde{E}_0(x)$ is maximum. Therefore, the coefficient of electron energy diffusion $\overline{\nu D_\varepsilon}$ sharply increases for $\varepsilon > e\Phi_{sh}$ (Figs. 3 and 4). It follows from equations (10)–(12) that the kinetics of electrons is mainly governed by the form of the function $\overline{\nu D_\varepsilon}(\varepsilon)$. In the energy range $T^* < \varepsilon < \varepsilon_1$ (here ε_1 is the first threshold for inelastic collisions, and $T^* = 1/(d\ln F_0/d\varepsilon)$ is the effective electron temperature in the energy range in which inelastic collisions are essential), the right-hand side of equation (10) tends to zero, and the solution of (10) takes a simple form:

$$F_0(\varepsilon) = \Gamma_\varepsilon \int_{\varepsilon_1}^{\varepsilon} \frac{d\varepsilon'}{\overline{\nu D_\varepsilon}(\varepsilon')}, \qquad (20)$$

where Γ_ε is the flux in energy space, which is approximately constant at $T^* < \varepsilon < \varepsilon_1$. Since $dF_0/d\varepsilon = \Gamma_\varepsilon/\overline{\nu D_\varepsilon}(\varepsilon)$, the slope of the EDF is very different for $\varepsilon < e\Phi_{sh}$ and $\varepsilon > e\Phi_{sh}$, i.e., a two-temperature EDF is formed.

In order to demonstrate the effect described, we carried out calculations of the EDF in the local and nonlocal approximations. Figure 3 presents the EDF and the coefficients of electron diffusion in energy. The calculations were performed for helium discharge at $p = 0.1$ torr, $\omega = 13.56$ MHz, $L_0 = 3.35$ cm, and $j_0 = 8.8$ mA/cm^2. The solid lines present the solution obtained by using FS. The EDF plotted by the dashed line is calculated in the local approximation; the coefficient of electron diffusion in energy is calculated using the oscillating-field amplitude in the center of the discharge $\tilde{E}(x = 0)$ instead of the full profile of $\tilde{E}(x)$. Values of all (electron and ion) cross sections are taken from [8].

For energy $\varepsilon > e\Phi_{sh} \sim 10$ eV, the FS techniques gives a sharp increase in $\overline{\nu D_\varepsilon}$ (Figs. 3 and 4), and the peak of cold electrons is seen in the EDF. The ratio of the ion densities in the center of the discharge to that at the electrode is approximately equal to 30. When the local approximation is used, a sharp increase in $\overline{\nu D_\varepsilon}$ and, consequently, two-temperature structure of the EDF disappear.

3.2. The Character of Transition to a Peaked EDF Profile as the Current Increases

Numerical simulations carried out for Ar demonstrate a dramatic rearrangement of the EDF with increasing the current. The results of simulations and experimental data [14] on the average electron energy and central plasma density as functions of the current density are presented in Fig. 5.

When $j_{0cr} \sim 1$ mA/cm^2, the average electron energy decreases with increasing the current both in simulations and experiment, and a peak appears in the EDF. For a fixed current density above j_{0cr}, the calculation gives a steady-state solution only when *e–e* collisions are taken into account. If *e–e* collisions are neglected, and the current is fixed, the plasma density infinitely increases (in this case, the relaxation method is used, see Subsection 2.5), and the average electron energy approaches zero. Electron–electron collisions are described by the collision integral $\mathrm{St}_{ee}(F_0)$, which is introduced into the right-hand side of (10)

$$\mathrm{St}_{ee}(F_0) = \frac{d}{d\varepsilon}\left(\overline{(vD_\varepsilon)}_{ee}\frac{dF_0}{d\varepsilon} + \overline{(vV_\varepsilon)}_{ee}F_0\right),$$

$$(vV_\varepsilon)_{ee} = \frac{mv^3}{2n(x)}8\pi\nu_{ee}(v,x)\int_{e\Phi(x)}^{\varepsilon} d\varepsilon\frac{v}{m}F_0(\varepsilon),$$

$$(vD_\varepsilon)_{ee} = \frac{mv^3}{2n(x)}\frac{8\pi}{3}\nu_{ee}(v,x)$$

$$\times\left[\int_{e\Phi(x)}^{\varepsilon} d\varepsilon\frac{v^3}{m}F_0(\varepsilon) + \frac{v^3}{m}\int_{\varepsilon}^{\infty} d\varepsilon F_0(\varepsilon)\right],$$

where $\nu_{ee}(v, x) = \dfrac{4\pi e^4\Lambda_{ee}n(x)}{m^2v^3}$, $v = \sqrt{(2/m)(\varepsilon - e\Phi(x))}$, and Λ_{ee} is the Coulomb logarithm.

In the this stage of investigations, we restrict ourselves to consideration of a non-self-sustaining RFC discharge.

The set of equations for FS includes a number of fairly intricate processes. However, it is possible to single out two basic processes leading to a steady-state solution. The first one, which dominates in the self-sustaining discharge, is the coupling of the plasma density and ionization rate via changing the amplitude of the oscillating conduction field. The higher is the plasma density, the lower is the field amplitude and, consequently, ionization rate, and vice versa. For example, if the integral source $\int_0^x dx\langle I(x,t)\rangle$ in the equation of continuity for ions (13) is greater than the ion flux Γ_i, then the plasma density increases. This leads to a decrease in the ionization rate, because electron heating decreases.

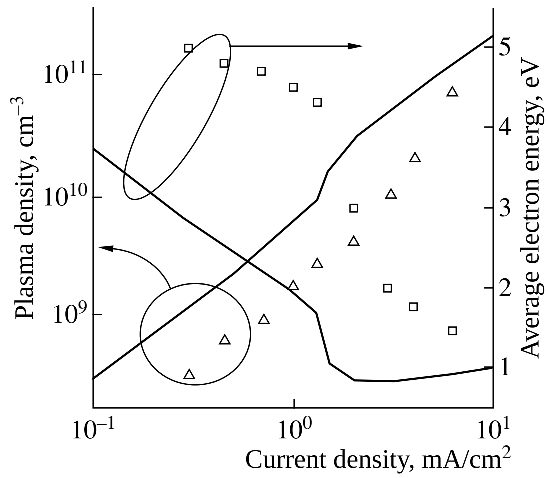

Fig. 5. Discharge in argon for $p = 0.1$ torr, $L_0 = 3.35$ cm, and $\omega = 13.56$ MHz. Average electron energy and plasma density at the center of the discharge as functions of the current density. Symbols (triangles and squares) correspond to experimental data [14]. The lines correspond to results of fast simulation with taking into account *e–e* collisions.

The second mechanism is the change of the ion flux due to a decrease in the ambipolar field, which is determined by average electron energy. An increase in the plasma density and decrease in the oscillating field result in the growth of the average lifetime of charged particles. In other words, an increase in the plasma density leads to an improvement of the plasma confinement, so that "self-trapping" (which was described in the Introduction and which is similar to the thermal explosion) becomes possible. In order to separate these two mechanisms, we first consider the simpler case, when the ionization source is fixed. Such a situation can occur in practice in the non-self- sustaining discharge. In the self-sustaining discharge, when ionization is determined by γ-electrons, whose free path is above the sheath thickness, ionization is more or less uniform in space and depends weakly on the amplitude of the oscillating field. In this case the second mechanism can dominate.

Thus, for the given ionization source, a single mechanism, which can provide the existence of a steady-state solution, is the change of the ion flux $\Gamma_i = n_iu_i$ due to the change of the ambipolar field. In the sheath, the ion density is independent of electron kinetics and is determined by the ionization rate (which is fixed) and voltage applied. In the center of the discharge, the rate of the ion escape is determined by the average energy of cold electrons and depends strongly on their kinetics. In this case, the higher the plasma density, the less the average energy of cold electrons, i.e., an increase in the plasma density results in a decrease in the rate of the ion escape from the central part of the discharge. Calculations show that a situation can occur when the resulting ion flux decreases or stays unchanged and

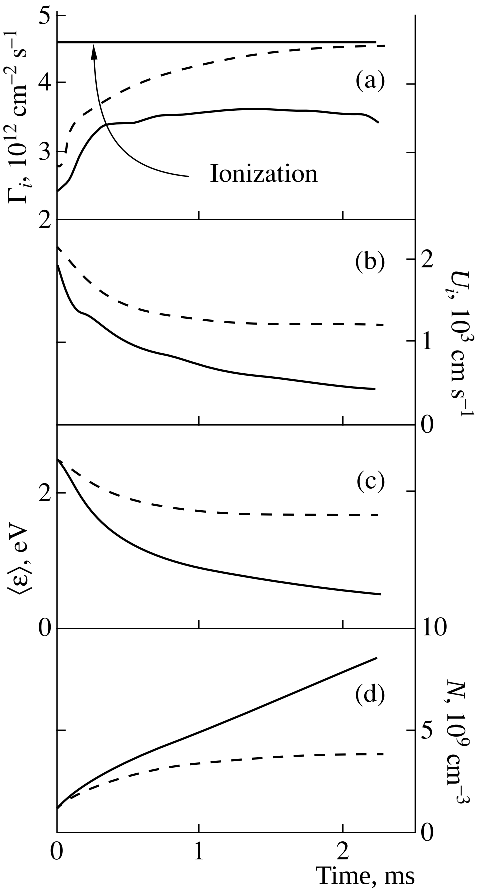

Fig. 6. Non-self-sustaining discharge in argon for p = 0.1 torr, j_0 = 0.3 mA/cm^2, L_0 = 3.35 cm, and ω = 13.56 MHz. The fixed ionization-source power corresponds to the doubled ionization-source power taken from the FS results for the same parameters. Time evolution of (a) the ion flux, (b) ion velocity, (c) average electron energy, and (d) plasma density at the point x^* = 0.3 cm. Solid lines are the results of calculation in the absence of the steady-state solution, when *e–e* collisions are not taken into account. Dashed lines are the results of calculations including *e–e* collisions. The thick line corresponds to $\int_0^{x^*} dx\langle I(x,t)\rangle$.

$\int_0^x dx\langle I(x,t)\rangle > \Gamma_i$, i.e., the plasma source power turns out to be higher than the loss power, and accumulation of the plasma occurs. For calculations with a fixed ionization source, we used a steady- state solution obtained in calculations of the argon self-sustaining discharge (p = 0.1 torr, j_0 = 0.3 mA/cm^2, L_0 = 3.35 cm, and ω = 13.56 MHz; *e–e* collisions are not included). Ionization source was doubled and fixed. Figure 6 shows the time evolution of the plasma density, ion velocity, average electron energy, and ion flux at the point x^* = 0.3 cm both with *e–e* collisions included (solid lines) and without them (dashed lines).

The initial values of the parameters correspond to the steady state obtained in calculations of a self-sustaining discharge. It is seen in Fig. 6 that, when *e–e* collisions are not taken into account, the stage of approaching a steady state (the ion flux approaches $\int_0^{x^*} dx\langle I(x,t)\rangle$, the solid line in Fig. 6a) is replaced with the stage in which an increase in the ion flux terminates. After that, the ion flux begins to decrease, because the plasma-density growth is balanced and even dominated by a decrease in the rate of the ion escape due to a decrease in the average electron energy. The effective electron temperature decreases from 2.5 eV to 0.5 eV. The steady state is not reached in this case. Including *e–e* collisions terminates a decrease in the average electron energy and provides the existence of a steady-state solution.

If *e–e* collisions are not taken into account, then, for $x < |L_p|$, the steady- state solution to the equation of continuity for ions (13) is absent. Let us consider equation (13) for $x < |L_p|$. We assume for simplicity that $e\Phi(x) = e\Phi(n(x))$ (actually, the EDF in equation (19) is an intricate function of both the potential and density). We also assume that $u_i = \mu(de\Phi/dx)$, which is a good approximation for small values of $\langle E\rangle/p$. For $x < |L_p|$, equation (13) is transformed to

$$e\mu\frac{d}{dx}\left[n\frac{dn}{dx}\frac{d}{dn}(\Phi(n))\right] = I(x), \qquad (21)$$

where $I(x)$ is the ionization source, which is fixed in our case. Assuming $I(x) = I_0$ = const, we can obtain the solution to equation (21)

$$\int_{n_p}^{n(x)} dnn\frac{d}{dn}[\Phi(n)] = \frac{I_0}{2e\mu}(L_p^2 - x^2). \qquad (22)$$

In obtaining (22), we used the boundary conditions $(dn/dx)|_{x=0} = 0$ and $n(L_p) = n_p$. It follows from (22) that the following relation must hold

$$\int_{n_p}^{n_0} dnn\frac{d}{dn}[\Phi(n)] = \frac{I_0}{2e\mu}L_p^2. \qquad (23)$$

All sheath parameters (including its density profile and the density n_p at the plasma boundary) are determined only by the ion flux from the plasma and are independent of the EDF and the potential profile in the plasma. Therefore, the quantity n_p in (22) can be regarded as fixed, and equation (22) can be used as equation for the plasma density n_0 in the center of the gap.

If, for example, $\Phi(n) \propto 1/n^\alpha$ with $\alpha > 1$, then the left-hand side of (23) increases with increasing n_0, but remains limited. Thus, for sufficiently large values of I_0, steady-state equation (21) has no solutions. This effect is similar to a thermal explosion when the temperature conductivity decreases with increasing temperature (see the Introduction).

Electron–electron collisions, which occur for a sufficiently high plasma density, lead to the heating of cold electrons due to their energy exchange with the fast ones, thereby, preventing a decrease in the average energy of the cold electrons. This corresponds to the transition to the case $\alpha = 0$.

The processes occurring in a self-sustaining discharge become more complex when it is necessary to incorporate self-consistent variations in the ionization rate. However, in this case, the electrons can also be broken into two groups with very different effective temperatures. The first group, with a total energy below the ambipolar potential at the sheath boundary, is heated by the oscillating field only slightly, whereas the second one, entering the sheath, is responsible for ionization.

The problem of a sharp transition to a peaked EDF profile in a self-sustaining discharge as the current increases is the subject of our further study.

ACKNOWLEDGMENTS

This work was supported in part by IAEA, contract no. 9238/R0/Regular Budged Fund.; INTAS, grant no. 96-0235; Naval Research Laboratory, contract no. 68171-97-M-5379; and Russian Foundation for Basic Research, project nos. 96-02- 16918, 98-02-16000 and 4391501 ("Export Technology and International Scientific Cooperation").

REFERENCES

1. Godyak, V. and Piejak, R., *Phys. Rev. Lett.*, 1990, vol. 65, p. 996.
2. Kaganovich, I.D. and Tsendin, L.D., *IEEE Trans. Plasma Sci.*, 1992, vol. 20, p. 66.
3. Berezhnoi, S.V., Kaganovich, I.D., and Tsendin, L.D., *Plasma Sources Sci. Technol.*, 1998 (in press).
4. Berezhnoi, S.V., Kaganovich, I.D., Levin, E.L., and Tsendin, L.D., *Proc. 10th Int. Conf. on Plasma Phys.*, Foz do Iguacu (Brazil), 1994, vol. 3, p. 9.
5. Berezhnoi, S.V., Kaganovich, I.D., and Tsendin, L.D., *Appl. Phys. Lett.*, 1996, vol. 69, p. 2341.
6. Landau, L.D. and Lifshitz, E.M., *Fluid Mechanics*, Oxford: Pergamon, 1987.
7. Smirnov, A.S. and Tsendin, L.D., *IEEE Trans. Plasma Sci.*, 1991, vol. 19, p. 130.
8. Raizer, Yu.P., *Gas Discharge Physics*, Berlin: Springer-Verlag, 1991.
9. Velikhov, E.P., Kovalev, A.S., and Rakhimov, A.T., *Fizicheskie yavleniya v gazorazryadnoi plazme* (Physical Phenomena in Gas-Discharge Plasmas), Moscow: Nauka, 1987, sec. 5.7.
10. Lieberman, M.A., *IEEE Trans. Plasma Sci.*, 1989, vol. 17, p. 338.
11. Lieberman, M.A. and Lichtenberg, A.J., *Principles of Plasma Discharges and Material Processing*, New York: Wiley, 1994.
12. Dmitriev, A.P. and Tsendin, L.D., *Zh. Eksp. Teor. Fiz.*, 1982, vol. 54, p. 1071.
13. Tsendin, L.D., *Zh. Tekh. Fiz.*, 1977, vol. 47, p. 925.
14. Godyak, V. and Piejak, R., *Plasma Sources Sci. Technol.*, 1992, vol. 1, p. 36; Godyak, V. and Piejak, R., personal communication.

Translated by A. D. Smirnova